Sequential Efficacy of Information for Optimized Geophysical and Drilling Strategies in Mineral Exploration

Peng Li[1], Jack Muir[2], Gerrit Olivier[2], David Zhen Yin[1], Jef Caers[1]

1. Mineral-X, Department of Earth & Planetary Sciences, Stanford University, USA
2. Fleet Space Technologies, Beverley, South Australia, Australia,

Corresponding author: Peng Li, Email: pli6@stanford.edu

This article has been submitted to *Geophysical Journal International* for publication. Please note that the manuscript has therefore not to be formally accepted for publication. Subsequent versions of this manuscript may have slightly different content. If accepted, the final version of this manuscript will be available via the "Peer-reviewed Publication DOI" link on the right-hand side of this webpage. Please feel free to contact us with any feedback.

Sequential Efficacy of Information for Optimized Geophysical and Drilling Strategies in Mineral Exploration

ABSTRACT

The global energy transition has created an urgent need for expanded critical mineral supply. Projected production from existing deposits and current discovery rates remains insufficient to meet this demand. More efficient exploration strategies are therefore required, particularly in optimizing costly and low-success data acquisition campaigns. To address this challenge, we introduce the concept of sequential Efficacy of Information (sequential EOI), a decision-making metric that quantifies the uncertainty reduction of target variables under proposed exploration action sequences. We demonstrate the framework using synthetic 2D and more realistic 3D porphyry copper systems, evaluating sequential combinations of exploration plans including ambient noise tomography (ANT) surveys and borehole drilling campaigns. With considering multiple experiments, including determining optimal borehole placement, optimizing ANT configurations, and comparing different action-ordering strategies, sequential EOI identified exploration plans that maximized the defined reward function. The method effectively revealed optimal designs such as dense ANT survey followed by large dip-angle borehole in the 2D case, and Pareto-optimal solutions under multi-criteria uncertainty metrics in 3D case. These results demonstrate that sequential EOI offers a practically meaningful foundation for multi-physics, multi-step, and uncertainty-driven plan optimization in mineral exploration, supporting rational decision-making under realistic operational constraints.

Keywords: optimal geophysical survey planning; hierarchical multi-step optimization; uncertainty reduction.

INTRODUCTION

The development of clean energy, transportation, and electronics depends highly on the discovery of critical minerals such as copper, nickel, lithium and cobalt. However, in recent decades, the success rate of finding a profitable deposit has declined heavily while the time consumed in the exploration phase has increased extensively (Sillitoe, 2010a; Koch et al., 2015; Okada, 2022). Industry and academic researchers are increasingly forced to deal with severe geological conditions such as deep subsurface or low-grade deposit areas to find more exploration zones. Consequently, more data acquisition actions are proposed and taken, and more iterations of target value evaluations are conducted, extending the exploration cycle and reducing the financial viability of early-stage mineral prospect development.

While much effort has been taken to use numerous methods and high-performance computing equipment to improve model prediction accuracy with the acquired data, less attention has been paid to question the rationale of the data acquisition plans, even though the costs of such plans are normally high while the success ratios are generally low. Such a "lookahead" problem is a decision-making or sequential decision-making process. In mineral exploration, such problems are challenging due to their multifaceted nature: not only does the evaluation of a plan in relation to subsurface models is needed, but also the evaluation between potential plans or sequential plans are needed, such that the optimal plan can be selected given an interested reward function. Taking the planning of drilling a borehole as an example, we are interested in assessing how the drilled borehole will contribute to improving our understanding about the geological system (this step can be done by doing inversion or geological analysis given the borehole information); we are also interested in where to drill the borehole, such that compared with other locations, the chosen location could provide maximum information about geological models (this step can be quantified

by defining a reward function and the goal is to maximize such reward function by choosing the optimal plan from options). An intuitive way to formulate the problem is a hierarchical learning setup. In this structure, an internal learning process is conducted in each possible plan space: given a proposed plan, we evaluate the information inside the plan and quantify the relationship between such information and subsurface model. Meanwhile, an outer learning process is conducted across all proposed plans: we evaluate the reward of taking each plan or sequence of plans and find the optimal action that maximizes the given reward, which supports the rationality of our decision-making principle.

Multiple methods can be adopted for the hierarchical learning structure. In geoscience applications, the inner learning step are generally related to inversions. Inversion approaches are widely used as a primary method for inferring subsurface information from indirect measurements in resource exploration. Traditional approaches typically rely on methods such as least-squares optimization (Aster et al., 2018; Menke, 2018; Tarantola, 2005), Markov chain Monte Carlo sampling (Mosegaard and Tarantola, 1995; Sambridge and Mosegaard, 2002; de Figueiredo et al., 2019; Li et al., 2021; Grana et al., 2022), and, more recently, deep neural networks (Das and Mukerji, 2020; Sun and Demanet, 2020; Li et al., 2024a, 2024b; Muir et al., 2024; Scheidt et al., 2025). The subsurface properties of interest may include petrophysical attributes (Stummer et al., 2002; Grana and Mukerji, 2015; Muir et al., 2022; Liu and Li, 2025), lithological parameters (Fouedjio et al., 2021; Yin et al., 2022), or geometric features (Muir and Tsai, 2020; Wei et al., 2024a), while the indirect observations often comprise geophysical measurements such as gravity (Li and Oldenburg, 1998), magnetic (Li and Oldenburg, 1996), electromagnetic (Cox et al., 2010; Oldenburg et al., 2020), borehole (Wei et al., 2024b; Yin et al., 2019), or ambient-noise data (Olivier et al., 2024, 2022; Reid et al., 2025), etc. However, the high dimensionality of geophysical data and the

nonlinearity of forward models often make these traditional techniques computationally prohibitive.

For the evaluation of exploration plans and actions, optimal experimental design approaches, with the aims of maximizing the information obtained from a minimum number of experiments, are widely adopted for fields including hazard monitoring networks (Maurer et al., 2010; Callahan et al., 2025), oil and gas (Box et al., 1978; Elvind et al., 1992), and mineral exploration (Stummer et al., 2002; Nazari et al., 2023). The idea of value of information (VOI) (Howard, 1966), which was inspired by ideas from decision theory (Raiffa and Schlaifer, 1961; Kochenderfer, 2015; Kochenderfer et al., 2022) has been widely adopted to evaluate action plans. The book by Eidsvik et al. (Eidsvik et al., 2015) provides background theory and extends the concept of VOI in spatial decision-making for different applications in geosciences including oil and gas, mining, and water resources management. Hall et al., (2022) proposed a method of sequential VOI to determine the optimal sequence and placement of exploration boreholes. However, the adopted VOI methods mostly measure the difference between prior models and posterior models given the proposed operation in the dollar value domain, where at each point, an economic model for mining is needed, thus may not be available in meaningful detail. A practical alternative to this challenge is the concept of Efficacy of Information (EOI) (Caers et al., 2022), which focuses on the domain of uncertainty reduction. EOI quantifies how much uncertainty of a variable of interest is reduced for a given proposal.

Mineral exploration is inherently a process of sequential decision-making under uncertainty. In practice, exploration teams follow an implicit “playbook” in which relatively inexpensive, large-scale data (e.g., potential-field geophysics or remote sensing) are used to identify areas of interest, after which increasingly diagnostic and costly methods (such as seismic, electromagnetic, or

drilling) are deployed. The information value of any single dataset is therefore context-dependent: it depends critically on what is already known. In early-stage exploration, economic pay-offs are uncertain and the goal is to maximize information gain through the optimal sequencing of geophysical surveys and drilling.

A seminal example of the importance of EOI concept in exploration is the discovery of Olympic Dam, South Australia, by Western Mining Corporation in 1975. The deposit was intersected in drillhole RD1, targeting a coincident gravity-magnetic anomaly beneath sedimentary cover (Porter, 2025). Following the discovery, numerous companies targeted similar potential-field anomalies across the Gawler Craton, expecting comparable mineralization. However, in the absence of an EOI-based framework to structure data acquisition and evaluate geological plausibility, most of these efforts were unsuccessful. Although a small number of campaigns achieved moderate success, such as the discovery of Carrapateena in 2005 (Porter, 2017), the vast majority were not. Many of the "look-alike" gravity and magnetic anomalies were later shown to arise from variations in basement topography rather than from iron-oxide alteration systems (Funk, 2013).

This history underscores two key ideas central to sequential decision-making in exploration. Firstly, the non-uniqueness of individual geophysical methods means that multiple subsurface configurations can reproduce the same anomaly (Li and Oldenburg, 1998). Without prior constraints on basement depth and relief, the potential-field response of a dense mineralized system cannot be distinguished from that of basement topography undulations. Secondly, and most importantly, the order in which data are acquired fundamentally determines their informativeness. Constraining cover thickness or basement geometry through seismic or electromagnetic methods can dramatically increase the EOI of a subsequent gravity survey. In such cases, the information

becomes valuable only when interpreted within a sequential framework that accounts for prior uncertainty reduction.

In this paper, we propose a framework of evaluating sequential decision-making problems using sequential Efficacy of information (sequential EOI). EOI measures how much uncertainty of a variable of interest is reduced for a given data acquisition proposal (Caers et al., 2022). Maximizing EOI for an action sequence therefore aims to produce the most uncertainty reduction (most increase in knowledge), decoupling geological understanding from direct consideration of costs or economic impact. This formulation may be more appropriate to the holistic decision-making process than VOI during early-stage exploration efforts, when development of a realistic economic model is intractable. Additionally, past applications of EOI have focused on limited applications to a single data type (typically drill logging), in this study, we extend EOI analysis to a holistic multi-physical exploration setting. Although this concept has been recognized qualitatively in exploration strategy, this study formalizes that intuition. By quantifying sequential EOI for alternative sequences of survey and drilling actions, we provide a decision-analytic basis for what practitioners have long done heuristically: deciding what to do next based on how much a proposed action is expected to reduce geological uncertainty. This framework therefore bridges traditional exploration workflows with quantitative measures of information efficacy.

The structure of this paper is organized as follows. In the methodology section, as a prelude to the EOI concept, we first introduce the ideas of VOI and sequential VOI in the binary case, followed by the transition from VOI to sequential EOI using probability density functions. We then present the mathematical formulations of sequential EOI and their corresponding implementation techniques. In the application section, we first demonstrate the method using a synthetic 2D example to illustrate the step-by-step computations, followed by a more realistic 3D case involving

additional variables and action options. Finally, we conclude the paper with an analysis of the 2D and 3D results.

METHODOLOGY

Efficacy of information for binary outcomes

In Caers et al. (2022), EOI is defined as a metric that quantifies by how much the proposed data acquisition is expected to reduce uncertainty, on average, on some property of interest. The EOI metric can be seen as a value of information metric without the need for an economic model. VOI can be represented by a decision tree, see Figure 1. This decision tree represents the choice between a base project and the option of taking additional information. In its most simple form, the base project is subject to binary uncertainty, and the data itself is a binary random variable that informs success vs failure. The input to this tree is the prior probability of success and the accuracy of the information modeled using a likelihood probability. In this framework, VOI is expressed as the difference between the base project value (PV) and the value of the information gathering branch or posterior value (PoV)

$$VOI = PoV - PV \tag{1}$$

Information is then gathered when VOI is more than the cost of the information. In EOI, $ values are not considered. Instead, the base project will return "1" in case of success and "0" in case of failure. The walk away option is now replaced by $P(A)$. In other words, in the base project, the value of go-ahead ($P(A)$) is equal to the value of walk away. As such, the decision maker has a choice of continuing with the current project or walking away to a project with similar prior chance

of success. Therefore, the third branch (acquire information) will be taken if gathering data will have a value larger than $P(A)$.

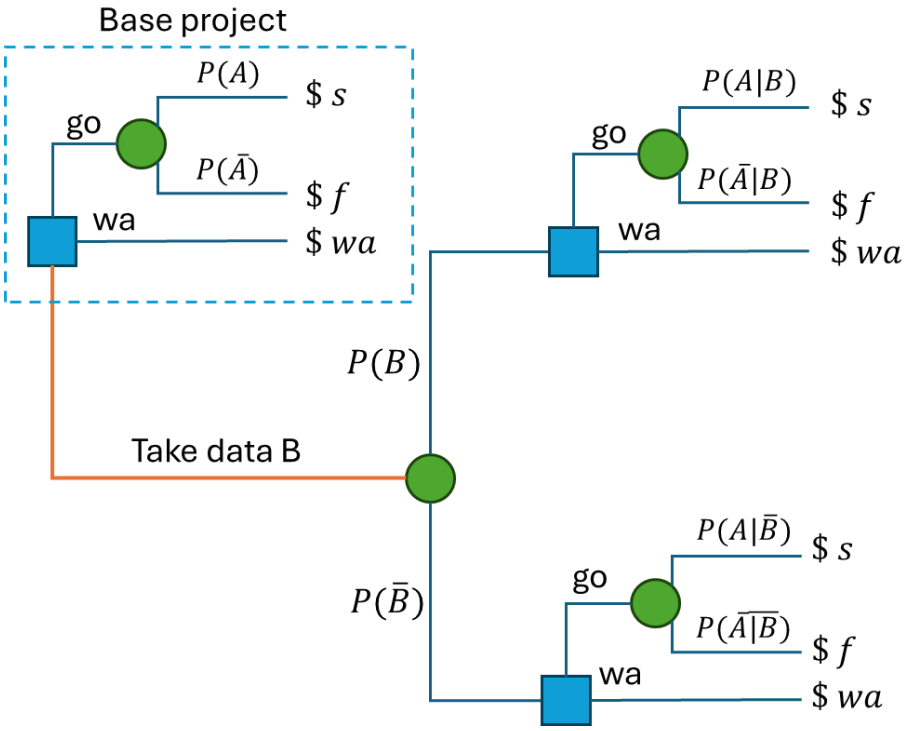

Figure 1: VOI expressed as a decision tree: $\$s$ is the return of a positive outcome, $\$f$ is the cost of a negative outcome and $\$wa$ is the return of walking away (usually equal to zero). In EOI, $\$s$ = 1, $\$f$ = 0, $\$wa$= P(A).

Sequential efficacy of information

Sequential value of information (sequential VOI) (Hall et al., 2022) concerns the assessment of the value of two information gathering campaigns that follow each other. The choice now lies between doing only the first campaign or having the option of continuing with the second campaign. In other words, the value of the first campaign is assessed including the possibility of a second. For example, one may drill a first borehole at a different location if we had the option of a second borehole compared to only considering one borehole. Sequential VOI is therefore different from two independent assessments of single VOIs. Like sequential VOI, one defines

sequential EOI and turns the sequential VOI decision tree into a sequential EOI decision tree, see Figure 2.

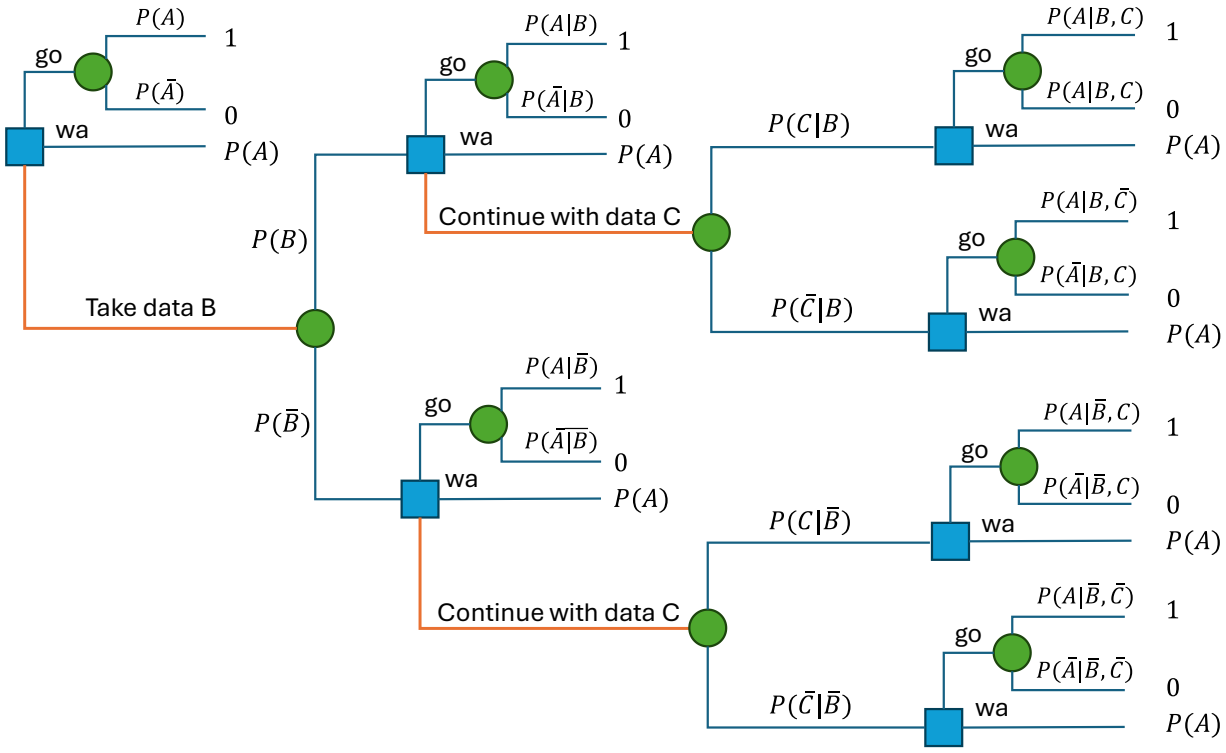

Figure 2: Sequential EOI, a (binary) data C is considered as an option after acquiring date B.

In this tree, we consider a second information source with a binary outcome that may inform success vs failure. After acquiring information B, we have the option to continue with information C, i.e. we don't have to. To solve this decision tree, we need, however, additional probabilities to be specified (input to the problem). First, we have the accuracy of the information C, i.e. the likelihood probability $P(C|A)$ for all outcomes of C and A, next we need $P(B,C|A)$ in order to calculate the posterior $P(A|B,C)$, again for all possible (8) outcomes of A, B, and C. The marginal $P(C|B)$ can be calculated from the posterior. In many cases, but not a requirement, a conditional independence assumption is made such as

$$P(B, C|A) = P(B|A)P(C|A) \quad (2)$$

In our implementation, we will not need this assumption.

Sequential efficacy of information with probability density functions

Real problems don't just use univariate binary or discrete variables. Geophysical and borehole data variables are vectors of information, containing a mix of discrete and continuous variables. Here we define EOI in this more general case through the use of a decision tree. In the general case, sums are replaced by integrals and probabilities by probability density functions, see Figure 3.

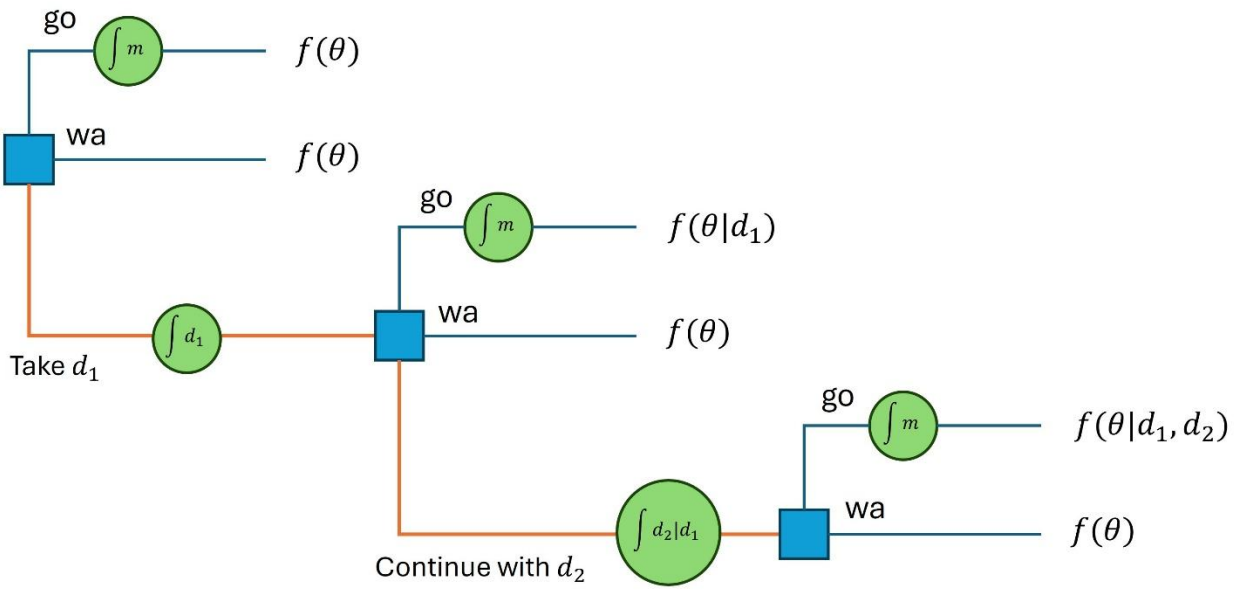

Figure 3: sequential EOI expressed using probability density functions.

In the base project we have a choice between $f(\theta)$ and $f(\theta)$, which is the equivalent as a choice between $P(A)$ and $P(A)$. θ is any vector with some properties of interest (e.g. grades vs tons for various cutoff grades). For probabilities of discrete events, we would always choose actions with

the highest probability of success. Here, we need a different metric. One possibility is to compare two densities using the KL-divergence. In this asymmetric metric one compares two densities $f_1(x)$ anf $f_2(x)$ as follows:

$$d_{KL}(f_2(x)||f_1(x)) = \int_x f_2(x) log\left(\frac{f_2(x)}{f_1(x)}\right) dx \tag{3}$$

This metric uses a log-ratio between densities. An appealing property of this metric is that the integral can be approximated by Monte Carlo simulation as follows:

$$d_{KL}(f_2(x)||f_1(x)) \cong \frac{1}{N}\sum_{n=1}^{N} log\left(\frac{f_2(x_n)}{f_1(x_n)}\right) \quad with \quad x_n \sim f_2(x) \tag{4}$$

In terms of the base project, we have

$$d_{KL}(f(\theta) \parallel f(\theta)) = \int_\theta f(\theta)\, log\left(\frac{f(\theta)}{f(\theta)}\right) d\theta = 0 \tag{5}$$

The metric ("posterior value") of only acquiring information d_1 is

$$EOI(\theta \parallel d_1) = \int_{d_1} d_{KL}\big(f(\theta|d_1) \parallel f(\theta)\big) dd_1 = \int_{d_1}\int_\theta f(\theta|d_1) log\left(\frac{f(\theta|d_1)}{f(\theta)}\right) d\theta \tag{6}$$

However, the option is available to acquire a second data d_2. Because d_2 is taken after d_1, we need to the integral of d_2 over all possibilities of d_1 (this is the equivalent of the $P(C|B)$ in Figure 2). The value to continue with d_2 ($\rightarrow d_2$) is

$$EOI(\theta, d_1| \rightarrow d_2) = \int_{d_2} f(d_2|d_1) \int_{\theta} f(\theta|d_1, d_2)\, log\left(\frac{f(\theta|d_1, d_2)}{f(\theta)}\right) d\theta dd_2 \quad (7)$$

However, this branch is only considered when that value is larger than Eq.6, hence the sequential EOI is defined as

$$EOI(\theta|d_1 \rightarrow d_2) = \int_{d_1} f(d_1)\, max\left\{EOI(\theta|d_1), EOI(\theta, d_1| \rightarrow d_2)\right\} dd_1 \quad (8)$$

The challenge now lies in approximating this value using Monte Carlo simulation. Any double integral will become a double sum. Also, all the density functions need to be known analytically, which is challenging in high-dimensional problems unless the distributions are Gaussian and the relationship between data and θ is linear. This is not the case for problems we consider; for example, the width of an alteration zone in a copper deposit is not linearly related to geophysical data. In the next section we will demonstrate in a simplified 2D case how we intend to make the MC approximations practical.

Monte Carlo approximation

To solve the sequential information gathering problem, we will approximate the integrals above using Monte Carlo simulation as follows. First, we need to sample prior model realizations to allow for the forward modeling of both data, namely

$$m^{(n)} \sim f(m), n = 1, \dots, N$$

$$d_1^{(n)} = g_1(m^{(n)})$$

$$d_2^{(n)} = g_2(m^{(n)}) \tag{9}$$

With g_1 and g_2 the forward model for both datasets. We consider the property or properties of interest θ to be some function of the model m,

$$\theta = h(m), \quad hence \quad \theta^{(n)} = h(m^{(n)}) \tag{10}$$

Using these samples, we approximate the EOI as follows

$$EOI(\theta \parallel d_1) \cong \frac{1}{N^2} \sum_{n=1}^{N} \sum_{n'=1}^{N} \log\left(\frac{f(\theta^{(n')}|d_1^{(n)})}{f(\theta^{(n')})}\right) \tag{11}$$

For a specific outcome $d_1^{(n)}$:

$$EOI\left(\theta \parallel d_1^{(n)}\right) \cong \frac{1}{N} \sum_{n'=1}^{N} \log\left(\frac{f\left(\theta^{(n')}\middle|d_1^{(n)}\right)}{f\left(\theta^{(n')}\right)}\right), \tag{12}$$

and,

$$EOI(\theta, d_1^{(n)}| \to d_2) \cong \frac{1}{N^2} \sum_{n'=1}^{N} \sum_{n''=1}^{N} \log\left(\frac{f(\theta^{(n'')}|d_1^{(n)}, d_2^{(n')})}{f(\theta^{(n'')})}\right) \tag{13}$$

With

$$d_2^{(n\prime)} \sim f(d_2|d_1^{(n)})$$

(14)

And finally

$$EOI(\theta|d_1 \to d_2) \cong \frac{1}{N}\sum_{n=1}^{N} max\left\{EOI(\theta, d_1^{(n)} \Vert\!\to d_2), EOI\left(\theta \parallel d_1^{(n)}\right)\right\}$$

(15)

In essence, we need to calculate a triple sum, over outcomes d_1, d_2 and θ. Detailed algorithm diagram can be seen in Appendix Algorithm 1.

Calculating probability density functions

Equation 11~15 calls for the calculation of density functions and the evaluation of the density function value in samples/outcomes. To circumvent high-dimensional functions, we will use an approach that combines machine learning with the concept of sufficient statistics (Schervish, 1995; Lehmann and Casella, 2005; Lehmann and Romano, 2022; Casella and Berger, 2024). In data science, a sufficient statistic is some function of the data that is sufficient to estimate a parameter of the distribution. For example, to estimate the mean of a distribution, based on a sample $x_1, x_2, \ldots x_N$ all we need to know is the statistic $\sum x_n$. It is as if we can replace the sample of size N with only one sum, which is the ultimate dimension reduction to 1D.

In our case, we deal with a similar situation, but our problem concerns a parameter θ and the data is a possibly high-dimensional vector (such as a geophysical dataset). To obtain a summary statistic in 1D for θ, we will train a neural network (non-linear function) that maps d into θ

$$\hat{\theta} = S_{ANN}(d) = S(d) \tag{16}$$

We train the neural network using the above Monte Carlo samples. To know whether S is a sufficient statistic, we need to plot $\hat{\theta}^{(n)} = S\left(d^{(n)}\right)$ versus the true θ. If we find that

$$\hat{\theta}^{(n)} = \theta + \varepsilon^{(n)} \tag{17}$$

with $\varepsilon^{(n)}$ a random error that is not function of θ, then the statistic is sufficient (Lehmann and Casella, 2005; Casella and Berger, 2024). The general rule is that the conditional distribution of $\hat{\theta}^{(n)}|\theta$ should not be function of θ. Note that this is also the case for $\sum x_n$ and the mean. What this basically means is that the ANN needs to fit the function S equally for various values of θ. Indeed, poorly fitting ANN would not be informative about θ.

Once the sufficiency of the statistics has been verified, the density estimation with a one dimensional θ, would be a three-dimensional problem in $\theta, S_1(d_1)$ and $S_2(d_2)$, which can be easily done using kernel density estimation (KDE) using the Monte Carlo samples (Appendix C). In all of the above expressions samples of d_1 and d_2 are replaced by samples of $S_1(d_1)$ and $S_2(d_2)$.

DEMONSTRATION ON A 2D PORPHYRY COPPER CASE

Case set-up

Porphyry copper deposits are a type of hydrothermal ore deposit, known for their large size and low to moderate copper grades, and are a major source of the world's copper (Donald A et al.,

2008). They are formed by the interaction of magmatic fluids with surrounding rocks, often associated with intrusions of felsic to intermediate composition (Richard H. Sillitoe, 2010; 2012). These deposits are characterized by extensive hydrothermal alteration, and a distinct zoning of alteration patterns. Mapping these alteration zones, especially those with potassic, phyllic, and propylitic alteration, can indicate the presence of a buried deposit. In terms of physical properties, Porphyry style deposits may have significant mechanical physical property differences to the surrounding host rock, in particular density variations associated with the underlying intrusion as well as significant seismic velocity gradients caused by brecciation and alteration during emplacement. For example, the prototypical Reko Diq porphyry complex in western Pakistan shows significant seismic velocity highs associated with intrusion into volcaniclastic host rock, including deep feeder features and broader, near-surface alteration halos (Razique, 2013; Jones et al., 2024). These features provide key information for identifying ore body using geophysical methods.

Before moving to a realistic 3D case, we use a simplified 2D model to illustrate the various concepts of sequential EOI and how practical calculations work. More specifically, we build a prior model of uncertainty which has four lithologies: intrusion, alteration, background rock and overburden, with each lithology having a distinct physical response (Figure 4.b). Generally, intrusions consist of diorite, granodiorite, and with variation in hydrous mafic mineral abundance, showing a relatively high velocity feature. Alteration zone as a result of magmatic fluid interaction with the background rocks, is the typical carrier for metals such as copper, molybdenum, gold and silver. The alteration zone shows a relatively slow velocity feature and is the main target for our predictions (Figure 4.b). In a real case, such prior uncertainty (prior to ANT & drilling) may be derived from stochastic inversion of gravity data (Athens and Caers, 2022).

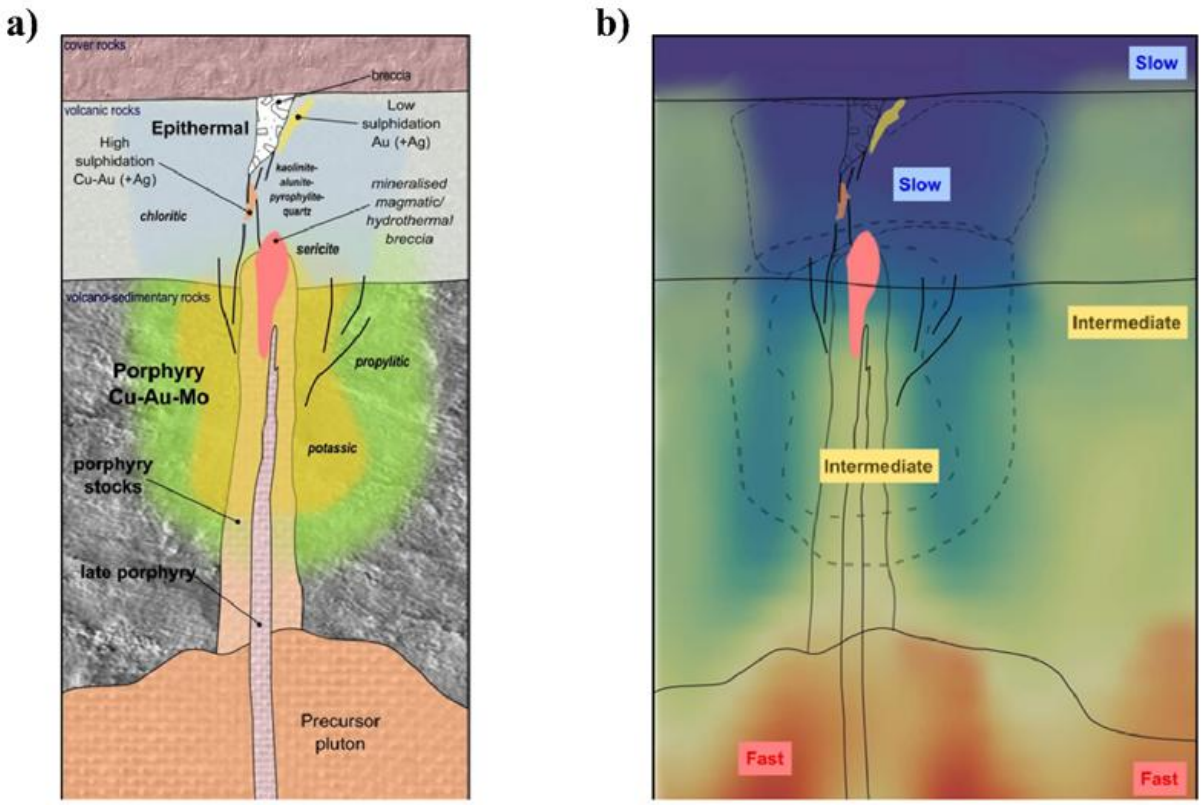

Figure 4: a) geological conceptual model of a porphyry copper deposit, modified from (Sillitoe, 2010; Hedenquist et al., 2012; Sillitoe, 2012); b) corresponding possible seismic velocity response. Warm color represents fast seismic velocity (borrowed from (Gal et al., 2024)).

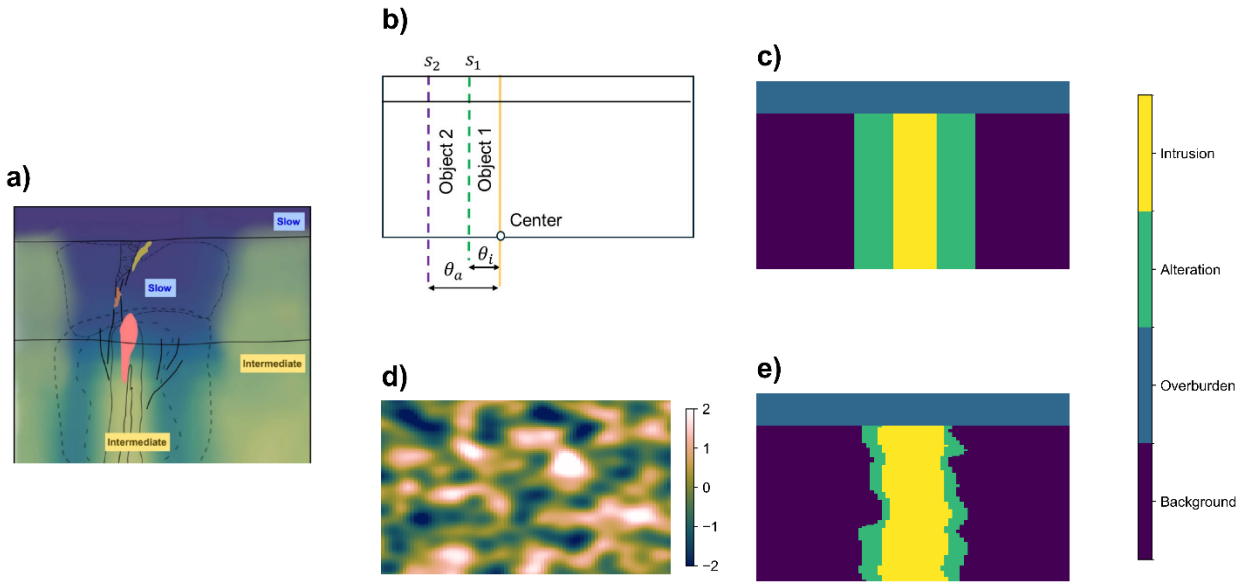

Figure 5: the process of prior modeling: a) establish the prior belief on existing data and known geological conditions, b) define variables to construct prior models: object 1 represents intrusion zone, with variable θ_i denoting intrusion width, object 2 represents alteration zone, with variable θ_a denoting alteration width, c) generate initial model of objects and their surface boundaries. The surface boundaries are then functionalized and converted into signed distance functions (SDFs), d), create a realization of Gaussian noise model, and e) add the Gaussian noise model to each boundary SDF, producing a perturbated boundary surface. Detailed progress can be found in Appendix A.

To illustrate the calculation of sequential EOI, we construct a simple model inspired by porphyry copper deposit geometries. To achieve this, we rely on geometric parameters that define the various zones (intrusion, alteration, overburden and background) with a Gaussian noise model to add local variability, see Figure 5. Figure 5.e is one realization of the entire model. Multiple realizations can be generated using Monte Carlo simulation for sufficient statistical analysis. In Table 1, we list the various (prior) distributions of each parameter. In a real case, these distributions could be obtained by stochastic inversion of the exiting geophysical data (e.g., low-resolution gravity data).

Table 1: a broad prior distribution on model variables for 2D case, as an initial statement of uncertainty, where $U[\cdot]$ represents uniform distribution.

Prior variables		**Definition**	**Distributions**	**Source for prior uncertainty statement**
Intrusion width	θ_i	Width of intrusion zone, in meters	$U[50, 100]$	Based on the background knowledge of porphyry copper system
Alteration width	θ_a	Width of alteration zone, in meters	$U[100, 300]$	

We consider two data acquisition campaigns that will be carried out in sequence. First, we need to decide on the geometry of the ANT survey, then we need to decide on the dip angle of a borehole, from a fixed location. The question therefore is: would we adjust the survey geometry, knowing that a borehole will be drilled next, or wouldn't it matter?

Solution

The Monte Carlo procedure requires first sampling models m, then running the data forward model to create samples (Figure 7):

$$m^{(n)}, d_1^{(n)}, d_2^{(n)}, \theta^{(n)}, n = 1, \dots, N \tag{18}$$

d_1 refers to ANT, while d_2 refers to the borehole. In this case, we have two different geometries for d_1 and three different d_2, so a total of six combinations is possible, see Figure 6. We need to also show that artificial neural networks (ANN) provide sufficient statistics for the single

prediction parameter θ. In Figure 8, we show 5 scatterplots, one for each possible dataset. We observe that the relationship between S and θ is linear and that the spread around the linear relationship is fairly constant over the range of θ.

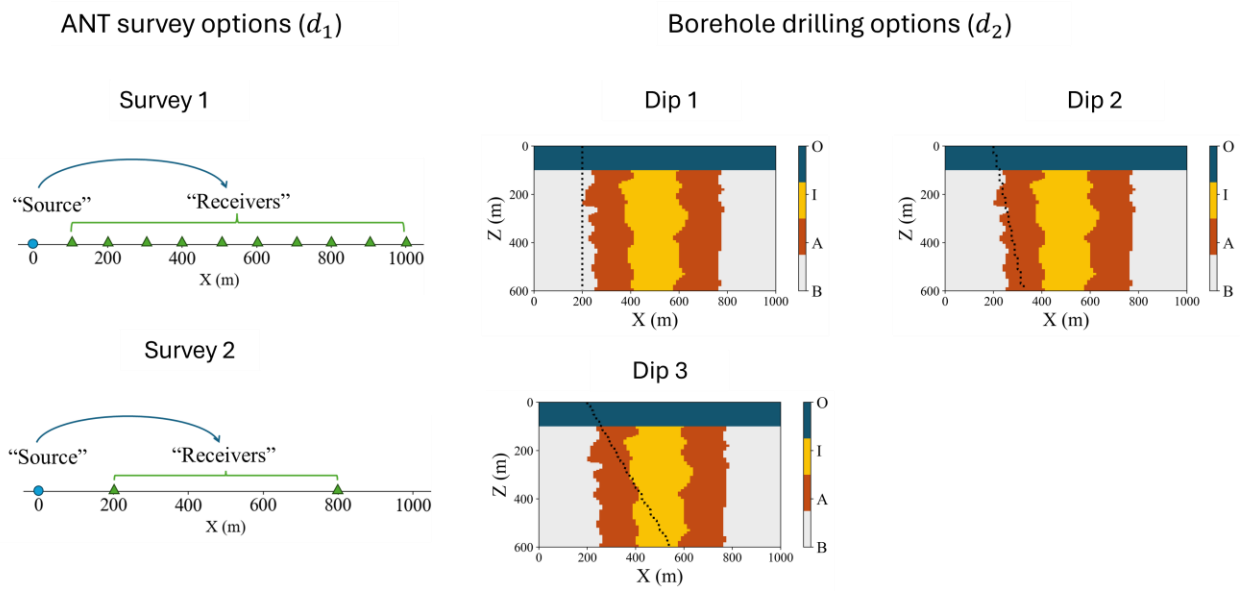

Figure 6: schematic design of two data acquisition plans. d_1 denotes the decision to conduct an ANT survey with two options: Survey 1 represents a dense survey plan; Survey 2 represents a sparse survey plan. d_2 denotes the decision to perform a borehole drilling from a fixed surface location with three options: Dip 1 represents a vertical borehole, Dip 2 a borehole a small dip angle, and Dip 3 represents a borehole a relatively large dip.

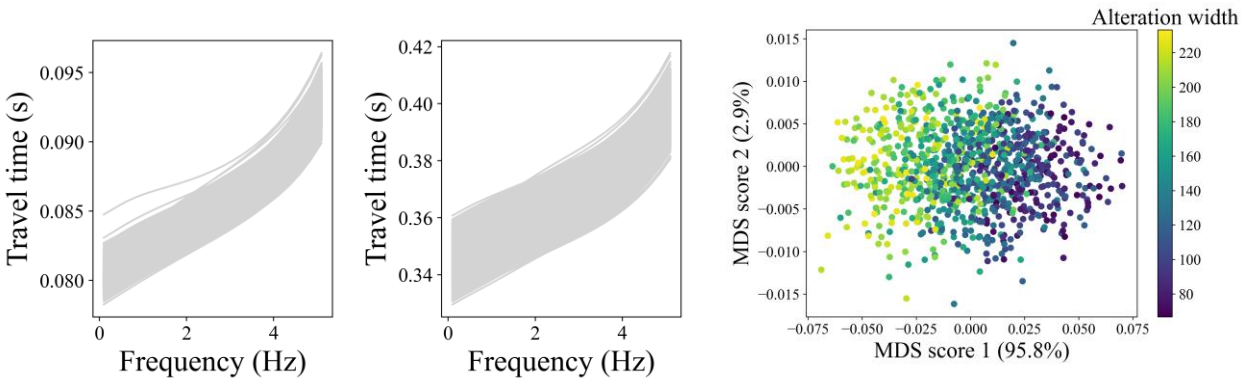

383

384 Figure 7: the signal simulation process (from Survey 2 in Figure 6) and dimension reduction conducted on

385 the generated signals. The MDS scatter plots are colored by the interested target.

386

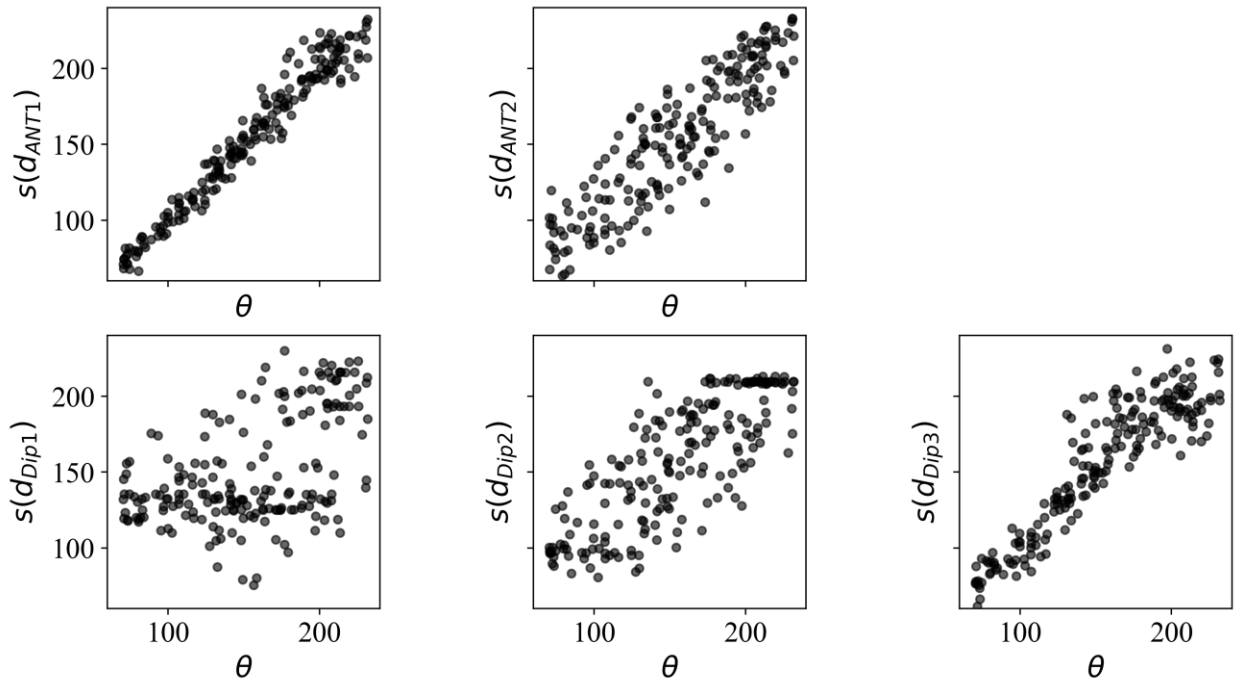

387

388 Figure 8: summary statistical relationship between θ and $\hat{\theta}$ (described in Equation 16) for all 5 plans. With

389 these statistical relations, the posterior probability density function and the following EOI and sequential

390 EOI can be calculated using Equation 11~ 15.

Figure 9 shows the EOI and sequential EOI for all sequential plans, calculated using Equation 11 ~ 15. The best plan is to acquire ANT in a dense configuration, then drill the borehole with dip3.

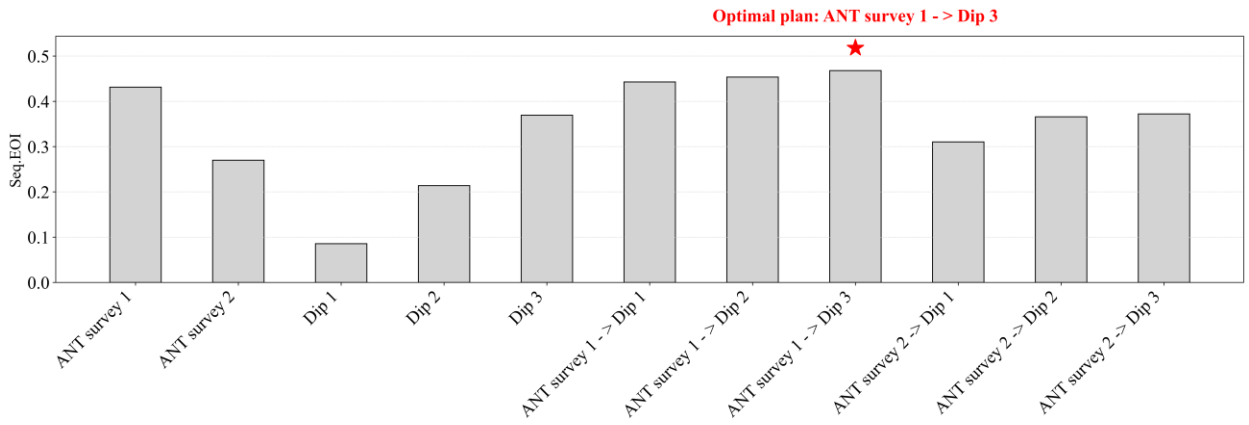

Figure 9: histogram of calculated EOI and sequential EOI from potential plans. The target variable in this case is the alteration width.

APPLICATION TO A 3D PORPHYRY COPPER CASE

Case description

We now consider a synthetic case that has several elements in common with what a real case would entail. In this real case setting, we have some prior knowledge about the geometry of porphyry copper system, known from geological understanding or analyzing the existing data, and the goal is to determine the planning of first an ANT survey, then possibly, follow up with drilling. The main question is: how do we design this survey, and where do we drill, in order to determine the location and extent of the economically relevant alteration zone that will likely contain the majority of mineralization convertible to reserve.

Based on this reference model, we assume a geological conceptual model of a porphyry copper deposit under an overburden, above a bedrock, with a main intrusion zone surrounded by alteration. This model represents a conceptually simplified view of the typical alteration sequence found in porphyry systems, focusing on the most economically relevant potassic alteration zone, and could be further extended (such as the collection of geochemical constraints from drilling are available) to include the full sequence of potassic-propylytic-phyllic-argillic of conceptual porphyry formation to capture detailed alteration and geochemical information at scales finer than can be resolved directly with geophysics. Quantitatively, we represent this conceptual model using objects whose boundaries are perturbed and assigned a constant but uncertain density and velocity. Figure 10 shows the comparison of reference model (Figure 10.a) and one realization (Figure 10.b) of prior models constructed using Monte Carlo simulation of the object-based modeling and perturbation method (detailed steps of prior model generations can be seen in Appendix A).

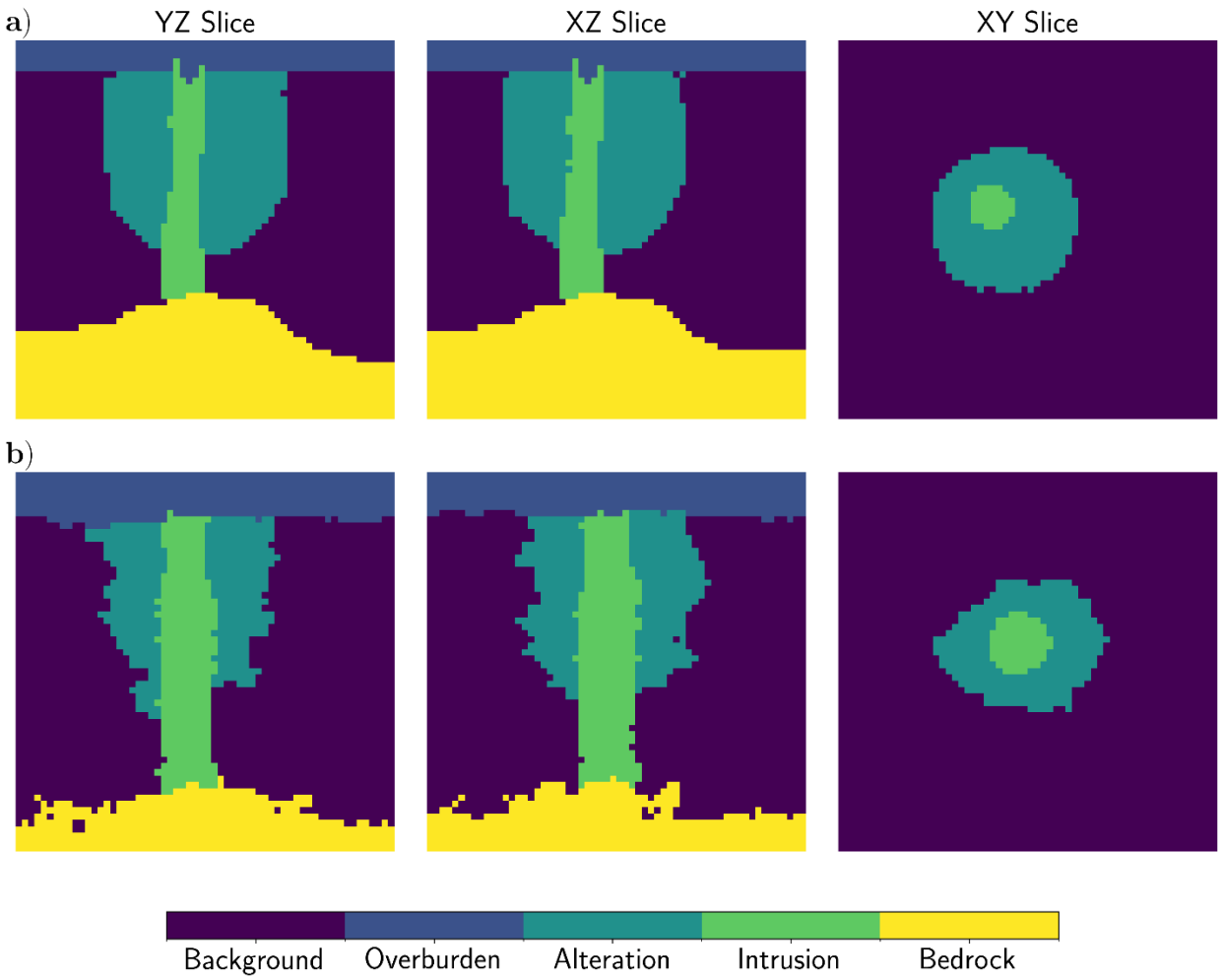

Figure 10: a) reference truth model, and b) a realization of prior model using object-based prior modeling method

Based on this prior modeling method, we can generate large number of prior models by sampling from the prior variable parameters. We start out with a wide prior (see Table 2). This prior could come from geological knowledge or could be inferred from Bayesian geophysical inversion of airborne geophysics (Caers, 2011). The resulting prior probability of having an alteration zone in the domain is large.

Table 2: prior distribution of model variables for 3D case, as an initial statement of uncertainty, where $U[\cdot]$ represents uniform distribution

Objects	Prior variables	Definition	Distributions	Source for prior uncertainty
Alteration	x_0	x coordinate of the ellipsoid center, in meters	$U[1250, 1750]$	based on the approximate target size and ellipsoid geometry definition
	y_0	y coordinate of the ellipsoid center, in meters	$U[1250, 1750]$	
	z_0	z coordinate of the ellipsoid center, in meters	$U[250, 750]$	
	a	semi-axes of the ellipsoid along x direction, in meters	$U[500, 1000]$	
	b	semi-axes of the ellipsoid along y direction, in meters	$U[500, 1000]$	
	c	semi-axes of the ellipsoid along z direction, in meters	$U[1000, 1500]$	
Intrusion	r	radius of the intrusion cylinder, in meters	$U[100, 250]$	based on the approximate target size and cylinder geometry definition
	h	height of the intrusion cylinder, in meters	$U[1750, 2750]$	
	x_0^i	x coordinate of the cylinder center, in meters	same location as alteration center x_0	
	y_0^i	y coordinate of the cylinder center, in meters	same location as alteration center y_0	
	z_0^i	z coordinate of the cylinder center, in meters	$z_0^i = h / 2$	
Overburden	t	thickness of the overburden soil, in meters	$U[250, 500]$	based on the background geology
Bedrock	d	depth of the bedrock surface, in meters	h	related to height of the intrusion

The prior modeling process results in realizations accounting for the current knowledge of the porphyry copper system before taking further actions. The decision to be made at this stage is either we go ahead / walk away, or we take further data for better understanding, even considering a second-round data acquisition if possible. Similar like the 2D case setup, we consider two data

acquisition campaigns that will be done in sequence. First, we need to decide on the geometry of the ANT survey, then we need to decide on the parameters for a borehole campaign.

Solution

The quantitative evaluation of a plan (e.g., an ANT survey design, a borehole design, or a sequence of designs) needs a criterion of interest, accounting for the numerical metric to help decision-makers to make rational decisions. In the 2D case, our criterion is the alteration width (a 2D version of volume), meaning that we evaluate each plan by quantifying how much uncertainty regarding alteration width would be reduced given the plan. In this realistic 3D case, we are interested in not only the total volume of alteration, but also the location of the ore body. To that end, we defined two objective axes: alteration volume and the surface center of alteration (i.e., prior variable of $[x_0, y_0]$ in Table 2), as our target of interests. The goal of sequential EOI then lies in quantifying which plan would provide maximum information toward these two targets jointly.

As illustrated in the 2D case, the calculation of EOI related to each plan requires four steps: first a plan is designed, secondly, the signals are generated from prior models based on the plan (i.e., forward simulation), thirdly, data processing and inversion step is conducted (e.g., dimension reduction and inversion using ANN) to align data and model variables, and finally, the EOI is calculated using the method in sequential EOI section and Equation 10 ~ 15. Figure 11 shows an example of such process. We first define a regular-spacing ANT survey (Figure 11.a), which is a common consideration in practice. We then collect the travel time per frequency channel per prior model realization and per sensor (Figure 11.b). At this point, the dimensions of data domain are quite large, for example, we generated 1000 prior models, and 16 sensors are designed in this plan, the ANT forward model have 25 frequency channels, and the signals (i.e., travel time) are pairwise

between sensors. A data dimension reduction is conducted using the traditional Multi-dimension Scaling (MDS) and colored by the target criterion (Figure 11.c), then the inversion is done using ANN. Finally, the EOI is calculated based on the defined equation, in this case the EOI is 0.4961.

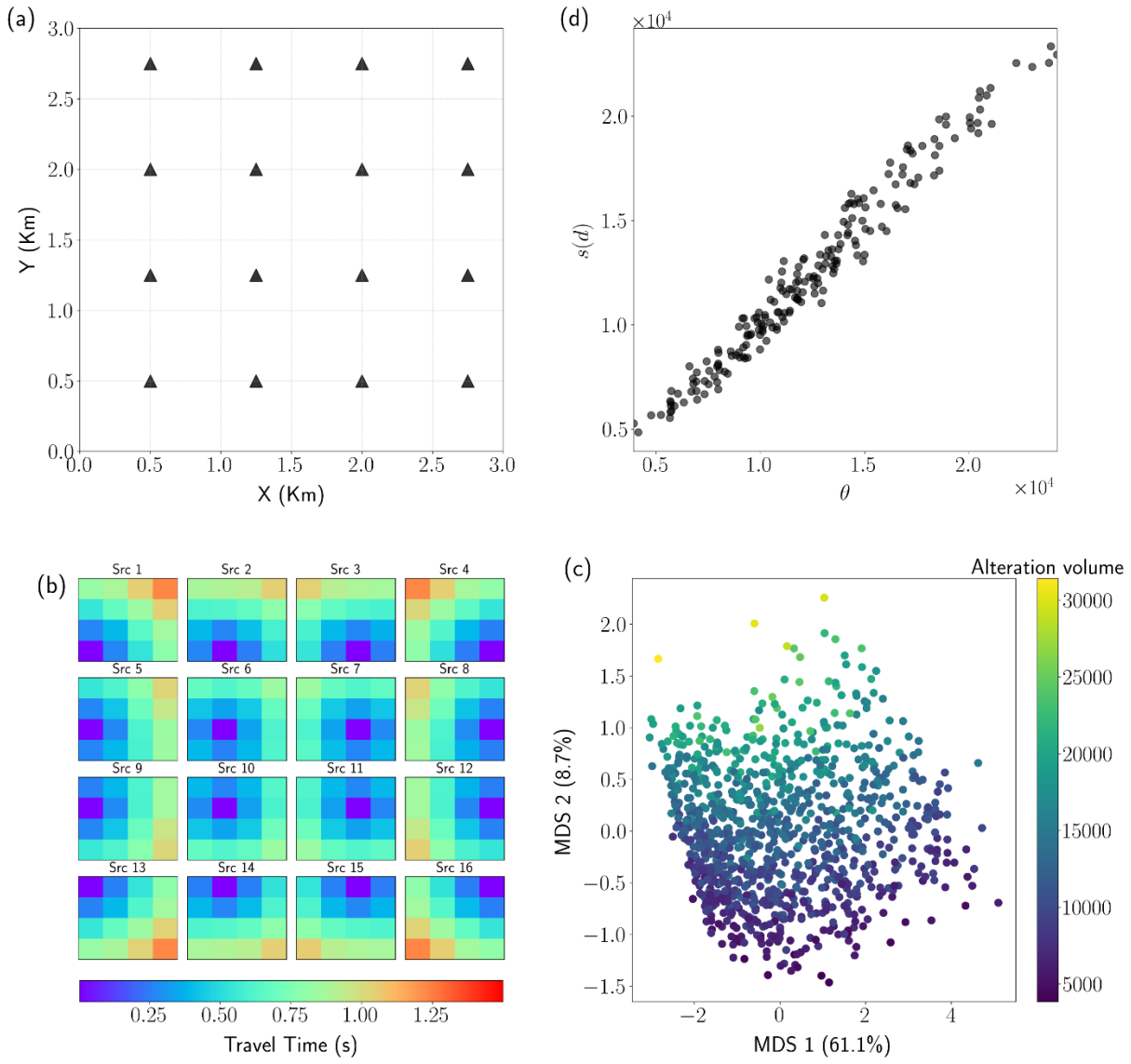

Figure 11: a workflow showing the steps of EOI calculation in 3D case: a) a schematic design of ANT survey, with equally distributed sensors, b) simulated signals based on prior models and designed survey, here we show the travel time of phase velocity of a given frequency channel, c) dimension reduction on

data space for fast inversion computation, and d) statistical relation between θ and $s(d)$, where posterior PDF and EOI can be calculated based on the relation.

Regarding the borehole campaign, the design of borehole path in 3D case would require more parameters compared to 2D case. Here we include 5 parameters for a borehole design (surface location $[x_0, y_0, z_0]$, dip angle, dip azimuth). Figure 12 shows one potential borehole plan. Compared to ANT survey evaluation, the borehole plan evaluation requires an intermediate step to transform the borehole lithological information (discrete) into continuous data. We use the method from (Caers et al., 2022), where after the transformation the borehole lithological information would be treated as continuous values, then the steps remain same as Figure 11.c and Figure 11.d. Detailed transformation can be seen in Appendix B

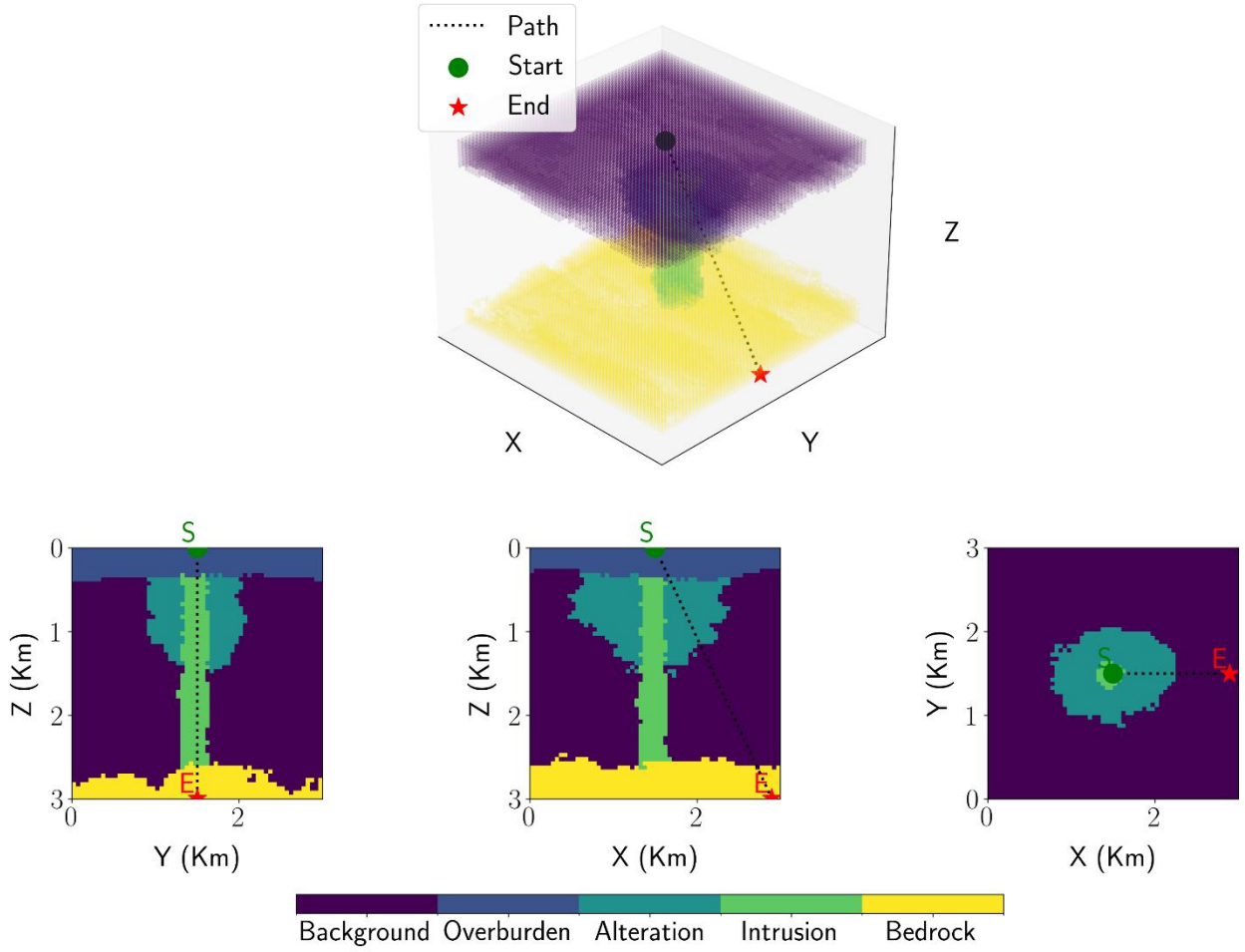

477

478 Figure 12: visualization of borehole design, the top row shows a 3D illustration of the borehole path, the
479 bottom row shows the borehole trajectory in 2D sections, “S” denotes the starting point, “E” denotes the
480 ending point.

481

482 Essentially, we can evaluate any possible ANT surveys and borehole plans applied on our prior
483 models. We select 3 ANT options and 3 borehole options for illustration simplicity but with
484 practical considerations. For example, the sensor spacing of sparse, medium, and dense ANT
485 surveys are 2000m, 750m, and 500m, accounting for the sensor spacing concerns; borehole 1 is
486 designed at the location with maximum alteration thickness (calculated from prior models),

borehole 2 is designed at the location with maximum alteration variance, and borehole is a borehole with a dip crossing the center of the alteration, accounting for common geological concern when drilling a borehole (Figure 13).

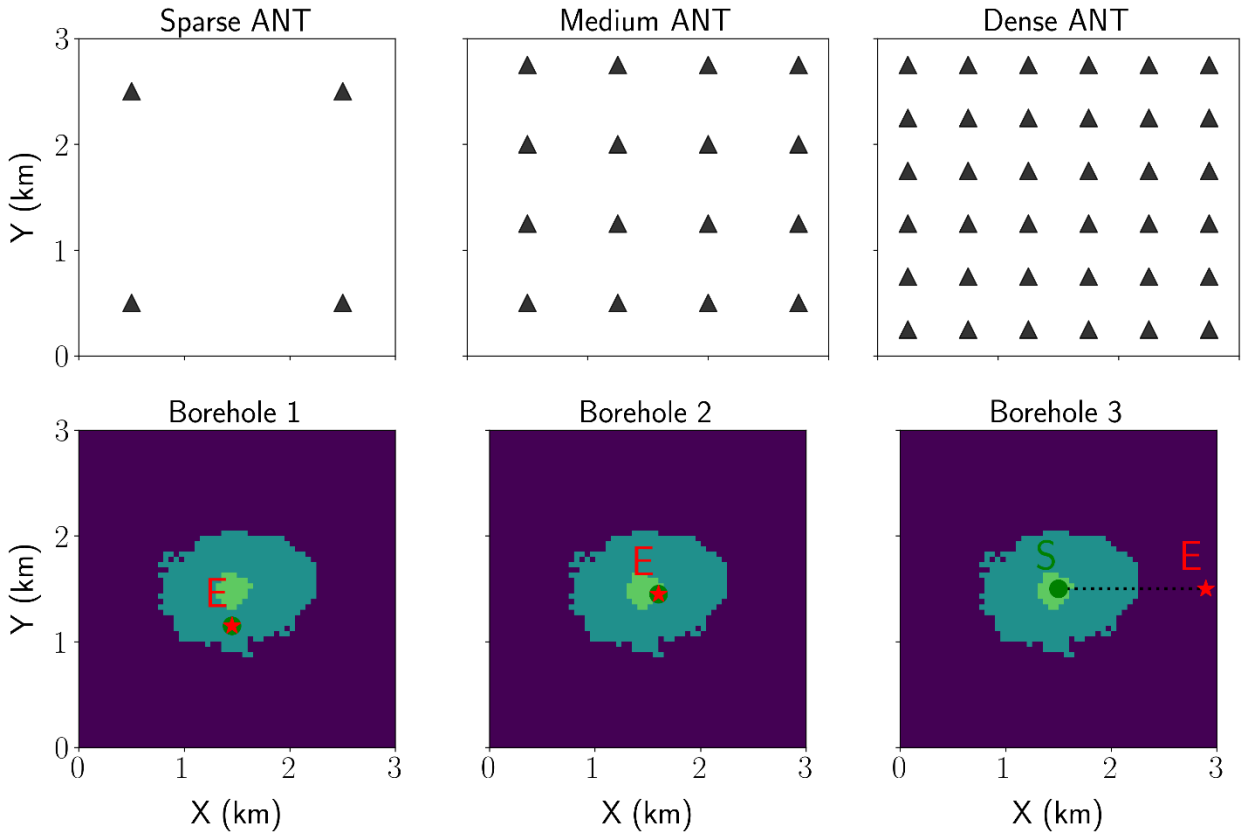

Figure 13: schematic design of ANT survey and borehole campaigns for 3D case. The top row shows the 3 options of ANT survey; the bottom row shows the three options of borehole drilling.

Similar to the 2D case shown in Figure 9, we can calculate the sequential EOI for the 6 plans and their sequential options given a criterion of interest. We can also calculate 2 or more criteria of interest and find the optimal solution by calculating the Pareto front of multiple objectives. Pareto front estimation for decision-making is a method for multi-objective optimization problems (Deb, 2004), where a set of non-dominated solutions could be selected as the optimal trade-off. Figure

14 shows the calculation of sequential EOI given two objectives: alteration volume and alteration center location $[x_0, y_0]$. The plot shows the optimal solutions identified by sequential EOI for each objective, as well as the "best" Pareto-front solution (Dense ANT followed by borehole 3), which enables decision-makers to evaluate both metrics simultaneously.

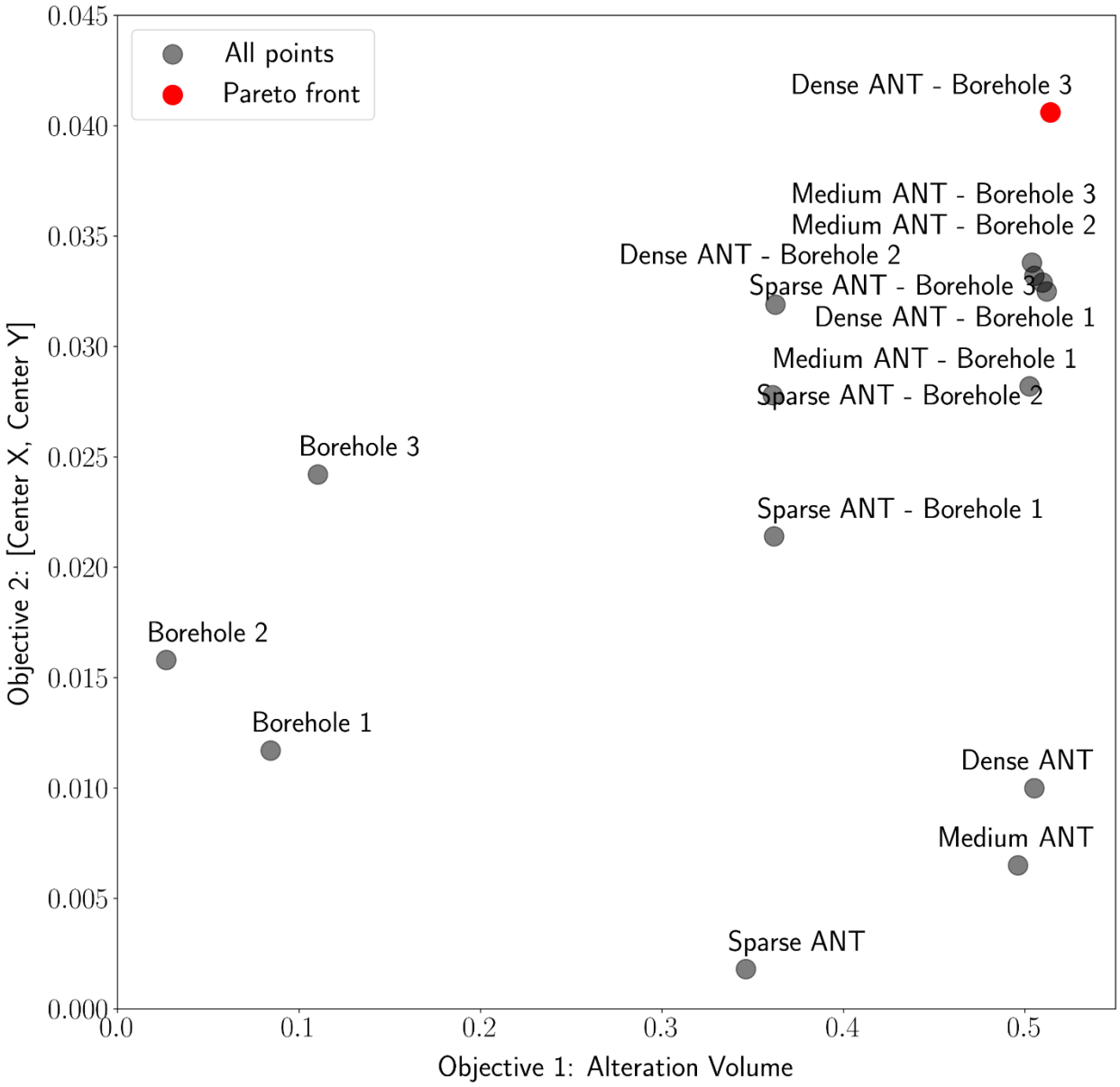

Figure 14: scatter plot of sequential EOI calculated from plans shown in Figure 13 for two targets of interest (two objectives), along with the calculated Pareto front. The Pareto front highlights the optimal options available to decision-makers.

CONCLUSION

We showed the concept of sequential EOI and its application as a decision-making metric for critical mineral exploration, particularly in the design of geophysical surveys (e.g., ANT), and borehole campaigns. Extended from the idea of EOI, sequential EOI aims to measure the uncertainty reduction of target variables under a proposed sequence of data acquisition plans, thereby providing a quantitative basis for rational exploration decisions. We illustrated the methodology using a synthetic 2D porphyry copper case and a more realistic 3D porphyry copper case. In 2D case, with the aim of reducing uncertainty about alteration width, we designed 2 ANT configurations and 3 borehole plans. The sequential EOI analysis identified that the dense ANT followed by a relatively large dip angle borehole would be the optimal option, effectively demonstrating the interpretability of the method. The 3D case extended the framework to a more realistic and complex setting, incorporating more model parameters with larger decision space, and multiple sequential EOI metrics. In this case, we use Pareto front to decide the optimal selection of the possible plans under multi-criteria conditions. Results from both 2D and 3D cases indicate that the sequential EOI framework produces practically meaningful outcomes, highlighting its potential to guide rational exploration planning decisions regarding uncertainty reduction. This approach establishes a foundation for multi-physics, multi-steps, and uncertainty-driven planning optimization in geoscientific decision-making, which could help decision-makers to make rational decisions under operational geoscience conditions.

ACKNOWLEDGMENTS

The authors acknowledge the support of Fleet Space Technologies, an industrial affiliate member of the Stanford Mineral-X Program, as well as the Stanford Mineral-X Program itself. The authors declare no conflicts of interest.

DATA AVAILABILITY STATEMENTS

The data and code underlying this article will be shared on reasonable request to the corresponding author.

REFERENCE

Aster, R.C., Borchers, B., Thurber, C., 2018. Parameter Estimation and Inverse Problems, 3rd ed. Elsevier.

Athens, N., Caers, J., 2022. Stochastic Inversion of Gravity Data Accounting for Structural Uncertainty. Math. Geosci. 54, 413–436. https://doi.org/10.1007/s11004-021-09978-2

Box, G.E.P., Hunter, W.G., Hunter, J.S., 1978. Statistics for experimenters: an introduction to design, data analysis, and model building, Wiley series in probability and mathematical statistics. Wiley, New York.

Caers, J., 2011. Modeling Uncertainty in the Earth Sciences. Wiley.

Caers, J., Scheidt, C., Yin, Z., Wang, L., Mukerji, T., House, K., 2022. Efficacy of Information in Mineral Exploration Drilling. Nat. Resour. Res. 31, 1157–1173. https://doi.org/10.1007/s11053-022-10030-1

Callahan, J., Monogue, K., Villarreal, R., Catanach, T., 2025. Analysis and optimization of seismic monitoring networks with Bayesian optimal experimental design. Geophys. J. Int. 240, 1802–1824. https://doi.org/10.1093/gji/ggae458

Casella, G., Berger, R., 2024. Statistical Inference, 2nd ed. Chapman and Hall/CRC, Boca Raton. https://doi.org/10.1201/9781003456285

Cox, L.H., Wilson, G.A., Zhdanov, M.S., 2010. 3D inversion of airborne electromagnetic data using a moving footprint. Explor. Geophys. 41, 250–259. https://doi.org/10.1071/EG10003

Das, V., Mukerji, T., 2020. Petrophysical properties prediction from prestack seismic data using convolutional neural networks. GEOPHYSICS 85, N41–N55. https://doi.org/10.1190/geo2019-0650.1

de Figueiredo, L.P., Grana, D., Roisenberg, M., Rodrigues, B.B., 2019. Gaussian mixture Markov chain Monte Carlo method for linear seismic inversion. GEOPHYSICS 84, R463–R476. https://doi.org/10.1190/geo2018-0529.1

Deb, K., 2004. Multi-objective optimization using evolutionary algorithms, Repr. ed, Wiley-Interscience series in systems and optimization. Wiley, Chichester Weinheim.

Donald A, S., Vladimir I, B., Barry C, M., 2008. Porphyry Copper Deposits of the World: Database and Grade and Tonnage Models (Open-File Report), Open-File Report.

Eidsvik, J., Mukerji, T., Bhattacharjya, D., 2015. Value of Information in the Earth Sciences: Integrating Spatial Modeling and Decision Analysis. Cambridge University Press, Cambridge.

Elvind, D., Asmund, H., Rolf, V., 1992. Maximum Information at Minimum Cost: A North Sea Field Development Study With an Experimental Design. J. Pet. Technol. 44, 1350–1356. https://doi.org/10.2118/23139-PA

Fouedjio, F., Scheidt, C., Yang, L., Achtziger-Zupančič, P., Caers, J., 2021. A geostatistical implicit modeling framework for uncertainty quantification of 3D geo-domain boundaries: Application to lithological domains from a porphyry copper deposit. Comput. Geosci. 157, 104931. https://doi.org/10.1016/j.cageo.2021.104931

Funk, C.W., 2013. Geophysical vectors to IOCG mineralisation in the Gawler Craton. ASEG Ext. Abstr. 2013, 1–5. https://doi.org/10.1071/ASEG2013ab242

Gal, M., Gerrit, O., Thomas, L., Grace, G., 2024. Assessing the Accuracy and Feasibility of Ambient Noise Tomography for Copper Exploration: Insights from Synthetic Data Generation with Realistic Geological Models. EGU General Assembly 2024, Vienna, Austria. https://doi.org/10.5194/egusphere-egu24-13672,%25202024

Grana, D., De Figueiredo, L., Mosegaard, K., 2022. Markov chain Monte Carlo for petrophysical inversion. GEOPHYSICS 87, M13–M24. https://doi.org/10.1190/geo2021-0177.1

Grana, D., Mukerji, T., 2015. Bayesian inversion of time-lapse seismic data for the estimation of static reservoir properties and dynamic property changes. Geophys. Prospect. 63, 637–655. https://doi.org/10.1111/1365-2478.12203

Hall, T., Scheidt, C., Wang, L., Yin, Z., Mukerji, T., Caers, J., 2022. Sequential Value of Information for Subsurface Exploration Drilling. Nat. Resour. Res. 31, 2413–2434. https://doi.org/10.1007/s11053-022-10078-z

Hedenquist, J.W., Harris, M., Camus, F., 2012. Geology and Genesis of Major Copper Deposits and Districts of the WorldA Tribute to Richard H. Sillitoe. Society of Economic Geologists. https://doi.org/10.5382/SP.16

Howard, R., 1966. Information Value Theory. IEEE Trans. Syst. Sci. Cybern. 2, 22–26. https://doi.org/10.1109/TSSC.1966.300074

Jones, T., Olivier, G., Murphy, B., Cole, L., Went, C., Olsen, S., Smith, N., Gal, M., North, B., Burrows, D., 2024. Real-Time Ambient Seismic Noise Tomography of the Hillside Iron Oxide–Copper–Gold Deposit. Minerals 14, 254. https://doi.org/10.3390/min14030254

Koch, A., Schilling, D., Upton, D., 2015. Tackling the Crisis in Mineral Exploration. AusIMM Bull. Oct 2015, 20–23.

Kochenderfer, M.J., 2015. Decision making under uncertainty: theory and application, MIT Lincoln laboratory series. The MIT press, Cambridge (Mass.).

Kochenderfer, M.J., Wheeler, T.A., Wray, K.H., 2022. Algorithms for decision making. MIT Press, Cambridge, Mass.

Lehmann, E.L., Casella, G., 2005. Theory of point estimation, 2. ed., [repr.]. ed, Springer texts in statistics. Springer, New York, NY Berlin Heidelberg.

Lehmann, E.L., Romano, J.P., 2022. Testing Statistical Hypotheses, Springer Texts in Statistics. Springer International Publishing, Cham. https://doi.org/10.1007/978-3-030-70578-7

Li, P., De Figueiredo, L., Grana, D., Mosegaard, K., 2021. Spatially correlated Markov chain Monte Carlo method for petrophysical inversion, in: First International Meeting for Applied Geoscience & Energy Expanded Abstracts. Presented at the First International Meeting for Applied Geoscience & Energy, Society of Exploration Geophysicists, Denver, CO and virtual, pp. 2139–2143. https://doi.org/10.1190/segam2021-3583101.1

Li, P., Grana, D., Liu, M., 2024a. Bayesian neural network and Bayesian physics-informed neural network via variational inference for seismic petrophysical inversion. GEOPHYSICS 89, M185–M196. https://doi.org/10.1190/geo2023-0737.1

Li, P., Liu, M., Alfarraj, M., Tahmasebi, P., Grana, D., 2024b. Probabilistic physics-informed neural network for seismic petrophysical inversion. GEOPHYSICS 89, M17–M32. https://doi.org/10.1190/geo2023-0214.1

Li, Y., Oldenburg, D.W., 1998. 3-D inversion of gravity data. GEOPHYSICS 63, 109–119. https://doi.org/10.1190/1.1444302

621 Li, Y., Oldenburg, D.W., 1996. 3-D inversion of magnetic data. GEOPHYSICS 61, 394–408.
622 https://doi.org/10.1190/1.1443968

623 Liu, Z., Li, Y., 2025. Connect Geophysical Data Interpretation and Geology Through Inversion
624 for Anisotropic Magnetic Susceptibility. Geophys. Prospect. 73, e70037.
625 https://doi.org/10.1111/1365-2478.70037

626 Maurer, H., Curtis, A., Boerner, D.E., 2010. Recent advances in optimized geophysical survey
627 design. GEOPHYSICS 75, 75A177-75A194. https://doi.org/10.1190/1.3484194

628 Menke, W., 2018. Geophysical data analysis: discrete inverse theory, 4th ed. ed. Academic press
629 an imprint of Elsevier, London.

630 Mosegaard, K., Tarantola, A., 1995. Monte Carlo sampling of solutions to inverse problems. J.
631 Geophys. Res. Solid Earth 100, 12431–12447. https://doi.org/10.1029/94JB03097

632 Muir, J., Olivier, G., Reid, A., 2024. End-to-End Mineral Exploration with Artificial Intelligence
633 and Ambient Noise Tomography. https://doi.org/10.48550/arXiv.2403.15095

634 Muir, J.B., Clayton, R.W., Tsai, V.C., Brissaud, Q., 2022. Parsimonious Velocity Inversion
635 Applied to the Los Angeles Basin, CA. J. Geophys. Res. Solid Earth 127, e2021JB023103.
636 https://doi.org/10.1029/2021JB023103

637 Muir, J.B., Tsai, V.C., 2020. Geometric and level set tomography using ensemble Kalman
638 inversion. Geophys. J. Int. 220, 967–980. https://doi.org/10.1093/gji/ggz472

639 Nazari, S., Rochlitz, R., Günther, T., 2023. Optimizing Semi-Airborne Electromagnetic Survey
640 Design for Mineral Exploration. Minerals 13, 796. https://doi.org/10.3390/min13060796

641 Okada, K., 2022. Breakthrough technologies for mineral exploration. Miner. Econ. 35, 429–454.
642 https://doi.org/10.1007/s13563-022-00317-3

643 Oldenburg, D.W., Heagy, L.J., Kang, S., Cockett, R., 2020. 3D electromagnetic modelling and
644 inversion: a case for open source. Explor. Geophys. 51, 25–37.
645 https://doi.org/10.1080/08123985.2019.1580118

646 Olivier, G., Borg, B., Trevor, L., Combeau, B., Dales, P., Gordon, J., Chaurasia, H., Pearson, M.,
647 2022. Fleet's Geode: A Breakthrough Sensor for Real-Time Ambient Seismic Noise
648 Tomography over DtS-IoT. Sensors 22, 8372. https://doi.org/10.3390/s22218372

649 Olivier, G., Heinson, G., Kay, B., Boren, G., Liu, Y., Carter, S., Jones, T., Dales, P., Abel, R.,
650 Vella, L., McAllister, L., 2024. Ambient noise tomography of an iron-oxide copper–gold
651 (IOCG) deposit under thick cover. Explor. Geophys. 55, 667–677.
652 https://doi.org/10.1080/08123985.2024.2371001

653 Porter, T.M. (Mike), 2025. PorterGeo dataset, Olympic Dam, OD Deeps.

654 Porter, T.M. (Mike), 2017. PorterGeo dataset, Carrapateena, Khamsin, Fremantle Doctor.

655 Raiffa, H., Schlaifer, R., 1961. Applied Statistical Decision Theory. Division of Research,
656 Graduate School of Business Adminitration, Harvard University.

657 Razique, A., 2013. Magmatic evolution and genesis of the giant reko diq h14-h15 porphyry
658 copper-gold deposit, district chagai, balochistan-pakistan. The University Of British
659 Columbia, Vancouver, BC, Canada.

660 Reid, A., Olivier, G., Jones, T., 2025. Ambient Noise Tomography: A Sensitive, Rapid, Passive
661 Seismic Technique for Mineral Exploration. SEG Discov. 17–26.
662 https://doi.org/10.5382/SEGnews.2025-140.fea-01

663 Sambridge, M., Mosegaard, K., 2002. Monte carlo methods in geophysical inversion problems.
664 Rev. Geophys. 40. https://doi.org/10.1029/2000RG000089

Scheidt, C., Mathieu, L., Yin, Z., Wang, L., Caers, J., 2025. Masked Autoregressive Flow for Geochemical Anomaly Detection with Application to Li–Cs–Ta Pegmatites Exploration of the Superior Craton, Canada. Nat. Resour. Res. 34, 1–22. https://doi.org/10.1007/s11053-024-10409-2

Schervish, M.J., 1995. Theory of Statistics, Springer Series in Statistics. Springer New York, New York, NY. https://doi.org/10.1007/978-1-4612-4250-5

Seabold, S., Perktold, J., 2010. Statsmodels: Econometric and Statistical Modeling with Python. Presented at the Python in Science Conference, Austin, Texas, pp. 92–96. https://doi.org/10.25080/Majora-92bf1922-011

Sillitoe, R.H., 2012. Copper Provinces. Soc. Econ. Geol. https://doi.org/10.5382/SP.16.01

Sillitoe, R.H., 2010a. The Challenge of Finding New Mineral Resources: An Introduction. https://doi.org/10.5382/SP.15.1.01

Sillitoe, R.H., 2010b. Porphyry Copper Systems. Econ. Geol. 105, 3–41. https://doi.org/10.2113/gsecongeo.105.1.3

Stummer, P., Maurer, H., Horstmeyer, H., Green, A.G., 2002. Optimization of DC resistivity data acquisition: real-time experimental design and a new multielectrode system. IEEE Trans. Geosci. Remote Sens. 40, 2727–2735. https://doi.org/10.1109/TGRS.2002.807015

Sun, H., Demanet, L., 2020. Extrapolated full-waveform inversion with deep learning. GEOPHYSICS 85, R275–R288. https://doi.org/10.1190/geo2019-0195.1

Tarantola, A., 2005. Inverse Problem Theory and Methods for Model Parameter Estimation. Society for Industrial and Applied Mathematics. https://doi.org/10.1137/1.9780898717921

686 Wei, X., Sun, J., Sen, M., 2024a. 3D Monte Carlo geometry inversion using gravity data.
687 GEOPHYSICS 89, G29–G44. https://doi.org/10.1190/geo2023-0498.1

688 Wei, X., Yin, Z., Scheidt, C., Darnell, K., Wang, L., Caers, J., 2024b. Constructing Priors for
689 Geophysical Inversions Constrained by Surface and Borehole Geochemistry. Surv.
690 Geophys. 45, 1047–1079. https://doi.org/10.1007/s10712-024-09843-x

691 Yin, Z., Amaru, M., Wang, Y., Li, L., Caers, J., 2022. Quantifying Uncertainty in Downscaling of
692 Seismic Data to High-Resolution 3-D Lithological Models. IEEE Trans. Geosci. Remote
693 Sens. 60, 1–12. https://doi.org/10.1109/TGRS.2022.3153934

694 Yin, Z., Strebelle, S., Caers, J., 2019. Automated Monte Carlo-based Quantification and Updating
695 of Geological Uncertainty with Borehole Data (AutoBEL v1.0).
696 https://doi.org/10.5194/gmd-2019-232

697

Appendix

A: Object-based prior modeling

The object-based prior modeling approach is designed to construct plausible prior lithological models by perturbing parameterized object boundaries, thereby accommodating the irregular and heterogeneous geometries of ore bodies. Object boundaries are represented using a level-set formulation, which enables flexible deformation while preserving topological consistency. We use the 3D porphyry copper case to demonstrate the steps of this method.

Guided by the prior geological understanding, an initial conceptual model is assembled through the combination of multiple parameterized geometric objects. In our 3D case, four objects are defined to represent key geological features: overburden (cubic geometry), alteration zone (semi-ellipsoidal geometry), intrusion (cylindrical geometry), and bedrock (cubic geometry). These components are subsequently integrated to construct the initial geological model (Figure A.1).

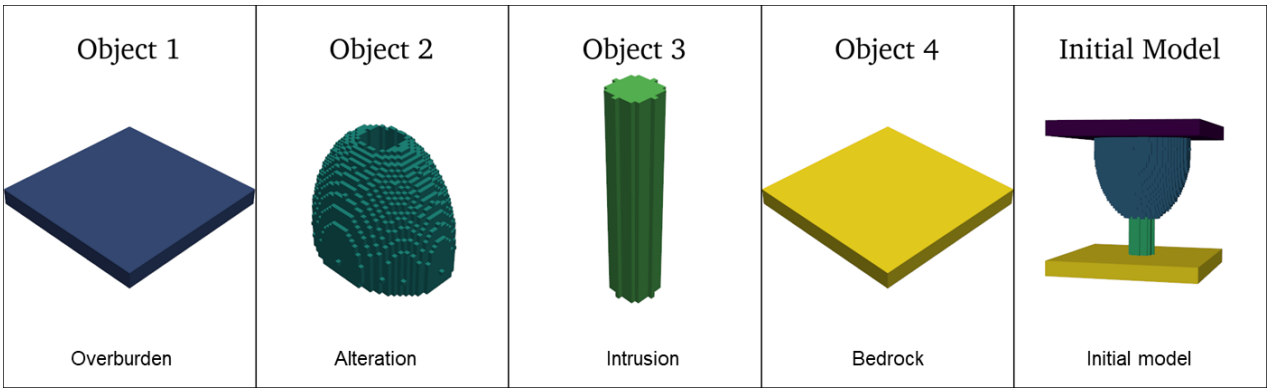

Figure A.1: four objects to represent key features of geological model

The perturbation of each object includes 4 steps, here we use alteration as an example:

- Define the object (i.e., ellipsoid) and sample object parameters from their prior distribution.

- Define the surface function of the ellipsoid

$$\left(\frac{x - x_0}{a}\right)^2 + \left(\frac{y - y_0}{b}\right)^2 + \left(\frac{z - z_0}{c}\right)^2 = 1 \quad \text{(A.1)}$$

Where x, y, z are the point coordinates, x_0, y_0, z_0 are the center coordinates, a, b, c are semi-axis length along 3 directions.

- Design the signed distance function (SDF) of the object.

$$SDF(object\ 2) = \left(\frac{x - x_0}{a}\right)^2 + \left(\frac{y - y_0}{b}\right)^2 + \left(\frac{z - z_0}{c}\right)^2 - 1 \quad \text{(A.2)}$$

By definition, an SDF has the properties of:

$$SDF(object\ 2)\begin{cases} < 0, if\ point\ inside\ object\ 2 \\ = 0, if\ point\ on\ surface \\ > 0, if\ point\ ourside\ object\ 2 \end{cases} \quad \text{(A.3)}$$

- Perturbate surface SDF by adding a 3D gaussian model noise. The 3D gaussian model noise can be generated using a gaussian process algorithm with some pre-defined parameters.

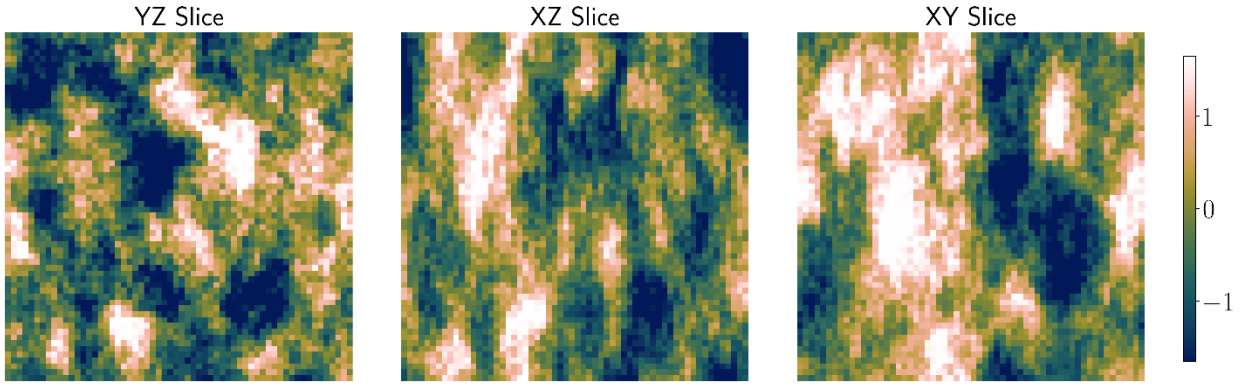

Figure A.2: 3 slices of one 3D gaussian model noise from different axis, with mean as 0.

For each object, boundary perturbations are applied using identical procedure. The perturbed objects are subsequently assembled to produce a single realization of the prior geological model. By performing Monte Carlo simulation, multiple realizations can be generated, thereby characterizing the uncertainty associated with subsurface geological structures. This method allows explicit boundary definition for level-set calculations and tunable level of geometric perturbation by adjusting the perturbation ratio assigned to each object. Moreover, as geophysical data are subject to volumetric averaging, small discontinuities introduced during perturbation exert negligible influence on the modeled geophysical response, ensuring that variability is expressed at scales resolvable by the data.

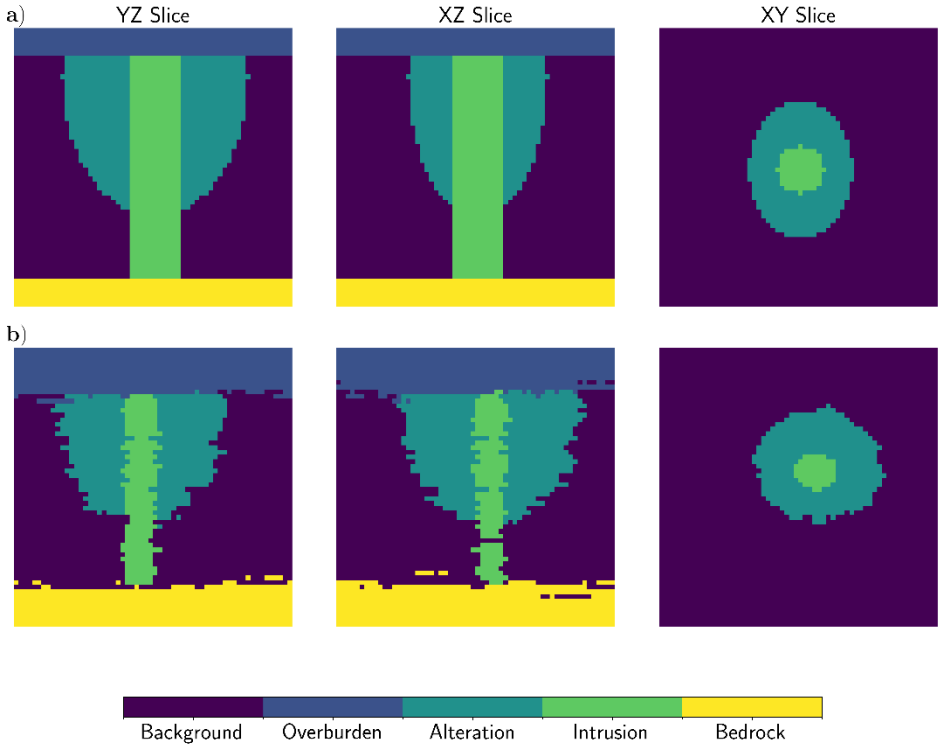

Figure A.3: comparison with initial model (a) and generated prior realizations (b).

B: Borehole lithological data transformation

We use borehole lithological information as a soft constraint on the prior models. Unlike geophysical data, which are typically continuous, lithological data are discrete and categorical. To incorporate this type of information into the model belief updating, the lithological data must first be transformed into a continuous form, ensuring consistency with other geophysical sources of information.

The transformation of borehole lithological data into a continuous form includes four steps. We use the borehole dip 3 in the 2D case as an example (Figure B.1):

- Project the designed borehole path into a lithological realization and extract the lithological data along the borehole path (Figure B.1.a),
- Transform the lithological information into an indicator matrix, with target lithology as 1 and background lithology as -1 (Figure B.1.b),
- Transform the information into continuous using signed distance function (SDF), as mentioned in Equation A.3, negative values denote points inside the object, zero denotes on surface, and positive values represent points outside the object. In this case, the object refers to the background rock (Figure B.1.c),
- Apply a sigmoid function to the SDF-transformed values to normalize them into the range [0, 1] (Figure B.1.d).

$$sigmoid\ (x) = \frac{1}{1 + \ e^{-x}} \tag{B.1}$$

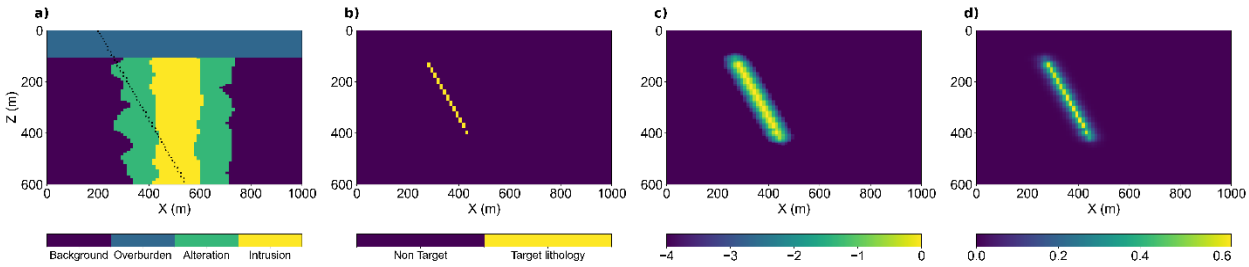

Figure B.1: Borehole lithological data transformation

The borehole lithology values are transformed into a continuous form, which can be used as indirect measurements for inversion. The same inversion method for geophysical data can be used. For more detailed information, we refer to (Caers et al., 2022).

C: Conditional Kernel Density Estimation (conditional KDE)

The posterior distribution of model parameters θ given the summary statistics $s(d)$ is expressed as

$$P(\theta|s(d)) = \frac{P(\theta, s(d))}{P(s(d))} \tag{C.1}$$

From the predictions of the neural network, we obtain $s(d)$, and with the corresponding label θ, the joint distribution $P(\theta, s(d))$ can be computed. For a single realization $s(d_i)$ of $s(d)$, the posterior distribution of the model parameters is given by

$$P(\theta|s(d_i)) = \frac{P(\theta, s(d_i))}{P(s(d_i))} \tag{C.2}$$

We use the conditional multivariate kernel density estimator $statsmodels.nonparametric.kernel\_density.KDEMultivariateConditional$ (Seabold and

Perktold, 2010) to implement the full calculation process. Figure C.1 shows an example of the calculation using the 2D case of ANT survey 2.

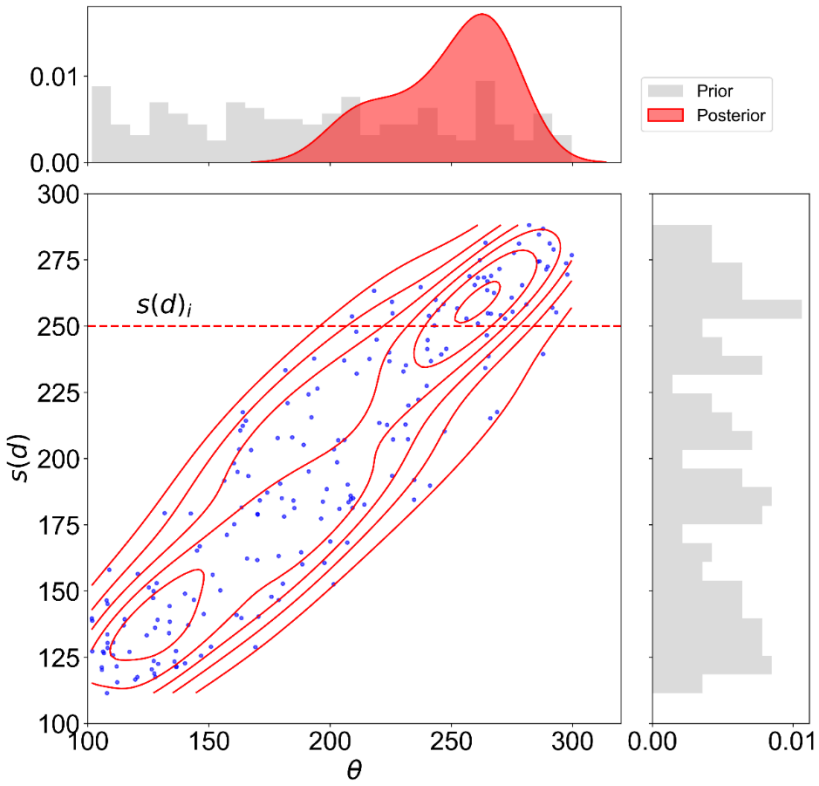

Figure C.1: the conditional kernel density estimation

Algorithm 1: Sequential EOI Computation

Input:

$f(\theta)$: Prior distribution for θ

$s(d_1)$, $s(d_2)$: Summary statistical dataset of d_1 and d_2

$f(\theta|d_1)$: Conditional distribution for θ given $s(d_1)$

$f(d_2|d_1)$: Conditional distribution for $s(d_2)$ given $s(d_1)$

$f(\theta|d_1, d_2)$: Conditional distribution for θ given $s(d_1)$ and $s(d_2)$

Output:

Sequential EOI: $EOI(\theta|d_1 \rightarrow d_2)$

Procedure:

1. Initialize $eoi\_list \leftarrow \emptyset$

2. For each sample d_1 in $s(d_1)$ do:

Step 1: $EOI\left(\theta \parallel d_1^{(n)}\right)$

(a) Draw posterior samples $\theta^{(n')}$ from $f(\theta|d_1^{(n)})$

(b) Compute log-ratio: $L_{n'} = log\,[f(\theta^{(n')}|d_1^{(n)})\,/f(\,\theta^{(n')})\,]$

(c) Compute $EOI\left(\theta \parallel d_1^{(n)}\right) = \frac{1}{N}\sum_{n'=1}^{N}(L_{n'})$

Step 2: $EOI(\theta, d_1^{(n)}| \rightarrow d_2)$

(d) Draw samples $d_2^{(n\prime)}$ from $f(d_2|d_1^{(n)})$

(e) For each $d_2^{(n\prime)}$ do:

i. Draw posterior samples $\theta^{(n'')}$ from $f(\theta^{(n'')}|d_1^{(n)}, d_2^{(n\prime)})$

ii. Compute log-ratio: $L_{n''} = log\,[\,f(\theta^{(n'')}|d_1^{(n)}, d_2^{(n\prime)})/\,f(\theta^{(n'')})]$

iii. Compute $EOI\left(\theta, d_1^{(n)}\middle| \rightarrow d_2^{(n\prime)}\right) = \frac{1}{N}\sum_{n''=1}^{N} L_{n''}$

(f) Compute $EOI\left(\theta, d_1^{(n)}\middle| \rightarrow d_2\right) = \frac{1}{N}\sum_{n\prime=1}^{N} EOI\left(\theta, d_1^{(n)}\middle| \rightarrow d_2^{(n\prime)}\right)$

Step 3: $EOI(\theta, d_1| \rightarrow d_2)$

(g) $EOI(\theta, d_1| \rightarrow d_2) = max\left\{EOI(\theta, d_1^{(n)} \nrightarrow d_2), EOI\left(\theta \parallel d_1^{(n)}\right)\right\}$

(h) Append $EOI(\theta, d_1| \rightarrow d_2)$ to eoi_list

3. Compute $EOI(\theta|d_1 \rightarrow d_2) \cong \frac{1}{N}\sum_{n=1}^{N} eoi\_list$

4. Return $EOI(\theta|d_1 \rightarrow d_2)$